The DLR Autonomous Navigation for the MMX Rover Under Phobos Environmental Influences: Illumination, Temperature, and Radiation

Lukas Burkhard[1] and Jitao Zheng[2] and Hans-Jürgen Sedlmayr[1]

***Abstract*— The Martian Moons eXploration (MMX) is set to examine the Martian Moons Phobos and Deimos. As part of this mission, a small rover named IDEFIX will explore the surface of Phobos as the first in situ system. The German Aerospace Center (DLR) develops the onboard autonomous navigation solution NAVDLR as a technology demonstration and also to increase the safety of rover driving operations. The harsh Phobos environment challenges the autonomous navigation due to its illumination conditions, the temperatures, and the radiation environment, especially as there remains a high uncertainty about the environmental parameters. This paper presents our approach to simulate varying and challenging environment effects on existing, representative data sets. We analyze the robustness of our autonomous navigation solution in relation to these conditions. Our results demonstrate that a loss of tracking can occur for challenging scenarios, but NAVDLR generally provides accurate and robust results. Finally, we propose mitigation techniques to reduce loss of tracking risk and improve navigation robustness.**

I. INTRODUCTION

The Martian Moons eXploration (MMX) will explore the Martian Moons Phobos and Deimos. It is a mission by the Japan Aerospace Exploration Agency (JAXA) and will be launched in 2026 with the aim of landing on Phobos in 2029 to collect samples and return them to Earth in 2031. The mission is outlined in [1] with the updated schedule provided by [2]. Part of this mission is a small rover named IDEFIX, which will be dropped from the MMX spacecraft prior to its landing to gather in situ information on the landing site and explore the surface of Phobos for approximately 100 Earth days [3]. The Centre National d'Etudes Spatiales (CNES) and the German Aerospace Center (DLR) provide the rover.

One challenge is the delayed communication between the rover and Earth, due to the data relay via the MMX spacecraft. A Phobos day (Phod) is approximately eight hours, but a communication round-trip can last multiple Phods to gather all relevant data. The delay motivates the usage of autonomous navigation algorithms to enable more efficient on-Phobos operations. To this end, DLR is developing the NAVDLR autonomous navigation solution that acts both as a technology demonstration by itself but also aims at enhancing operations by providing a range of functionalities from simple safety-stop on obstacle proximity to fully autonomous pathplanning features [4]. It uses IDEFIX's stereo navigation cameras for vision-based navigation and mapping.

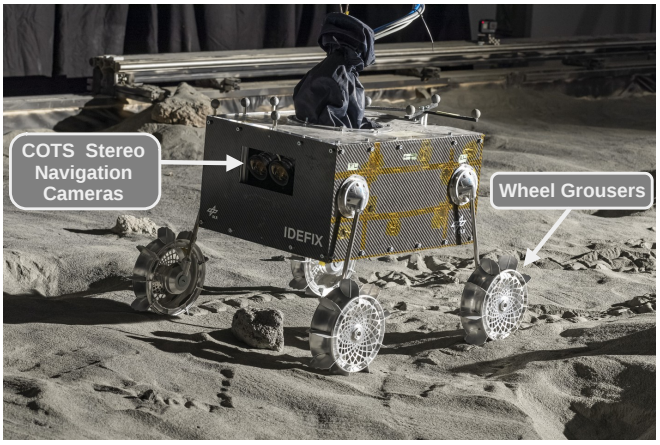

Fig. 1. The *Prototypix* platform for the IDEFIX rover in the DLR Planetary Exploration Laboratory (PEL).

One key challenge for NAVDLR is the conditions on Phobos. It is a very dark celestial body with no atmosphere, resulting in extreme temperature cycles and a high radiation environment [5]. Significant uncertainties remain on the precise parameters of the environment on the rover's scale due to a lack of previous scientific observations [5].

We describe the broad environment testing for NAVDLR in [6] and follow up on this here, where we study how the Phobos environment might compromise the camera observations and subsequently challenge NAVDLR's algorithms. Interestingly, little research is available on the performance of vision-based algorithms under such scenarios. Our contributions are therefore

- an initial study on how the robustness and accuracy of a vision-based navigation algorithm are affected by the influence of illumination, temperature, and radiation,
- the presentation of a baseline methodology to address this question in the future in detail
- and discussing potential mitigation strategies for failure cases to make the navigation more robust.

II. RELATED WORK

Multiple rover systems in the solar system rely on camera vision for operations and navigation. Early examples are the Mars Exploration Rovers Spirit and Opportunity, which pioneered the use of visual odometry on planetary

[1]Institute of Robotics and Mechatronics, German Aerospace Center (DLR), 82234 Wessling, Germany lukas.burkhard@dlr.de

[2]Department of Aerospace and Geodesy, Technical University of Munich (TUM), 85521 Ottobrunn, Germany

 DOI: https://doi.org/10.1109/iSpaRo66239.2025.11437357

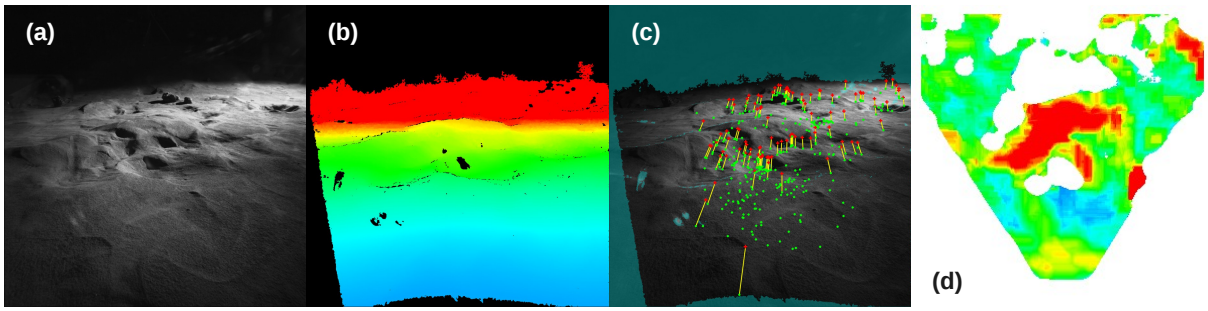

Fig. 2. The NAVDLR pipeline: 2048×2048 stereo images are binned to 1024×1024 and rectified (a); A depth image is computed by the SGM (b); Features are tracked over multiple images by the visual odometry VO to estimate the rover's pose (c); The depth information is used to create a map (d).

rovers [7]. Similarly, their follow-up missions, Curiosity [8] and Perseverance [9], leverage the visual odometry and hazard detection for efficient and partially autonomous rover operations. For Lunar rover operations, the Yutu-2 rover records images from the NavCams and computes elevation maps and pose estimation on Earth to aid teleoperations [10]. Similarly, the VIPER rover [11] will combine onboard navigation with on-ground computing.

Asteroids tend to be significantly darker than other celestial bodies, and similar conditions are expected for Phobos [12]. However, there have only been a few missions to such asteroids, with limited usage of optical autonomy methods. The OSIRIS-REx mission uses natural feature tracking to perform autonomous high-precision orbit determination as it tracks features on the asteroid Bennu and compares them to a stored database [13]. Lander systems on asteroids did take images – for example, the MASCOT lander on Ryugu [14] – but did not use vision-based navigation algorithms onboard.

The hostile space environment can negatively influence the performance of cameras. For the case of the MMX Rover, the corresponding CMOS chip [15] was extensively studied under the influence of radiation [16] to determine its robustness and the effects. To our knowledge, the mentioned missions or others have not published assessments on the influence of the environmental conditions of illumination and radiation on their autonomous navigation and mapping capabilities. This may be due to general disclosure constraints or because the risk is considered to be lower for Mars or the Moon. It also must be noted that in situ images from Mars and the Moon were available to test the navigation algorithms during development. This is missing in the case of Phobos, making the task more challenging.

Little research is available on how the space environment influences optical *algorithms*, especially for CMOS cameras. As a related example, [17] discusses the influence of radiation on event cameras and proposes a neural network for radiation event detection and corresponding mitigation strategies. The Pyxel tool [18] developed by ESA simulates all relevant environmental effects for cameras in space, including long-term radiation damage, short-term radiation effects, and the sensor's temperature variations while considering the underlying sensor type (i.e., CMOS or CCD).

III. THE AUTONOMOUS NAVIGATION NAVDLR

NAVDLR uses IDEFIX's stereo cameras to estimate the rover pose (the 3D position and 3D orientation combined), provide information on the environment as maps and as wheel slip estimation, and send commands to the rover's locomotion system. As it would exceed the scope of this work, we refer the reader to our previous work [4] for details on the NAVDLR software and to [6] regarding the general testing of NAVDLR.

A. Navigation Pipeline

The NAVDLR autonomous navigation pipeline consists of the following steps:

1) Receiving raw Bayer-Pattern 2048×2048 images from the left and right NavCams. These are demosaiced, rectified, and binned to obtain two monochrome 1024×1024 images (Fig. 2-a).
2) Dense depth image computation using the Semi-global Matching Algorithm (SGM) [19] (see Fig. 2-b), where the algorithm finds pixel correspondences between the left and the right camera image to compute the pixel's depth, given the $60\,\mathrm{mm}$ camera baseline and a given stereo camera calibration.
3) The visual odometry (VO) extracts features in the left camera images and tracks these during the rover motion (shown in Fig. 2-c) over the image sequence. This, together with the corresponding depth information, allows the estimation of the rover's six-dimensional pose over time. VO keeps a history of five images from the past as key frames to allow for a pose recovery in case of input images of questionable quality.
4) The following modules aggregate the depth information to an overall map over time. The maps are elevation models (digital elevation model - DEM) or obstacle maps that classify traversability (see Fig. 2-d). This is used to offer different levels of autonomy, starting from a simple safety stop due to critical proximity to a dangerous obstacle, to autonomous path planning and commanding.

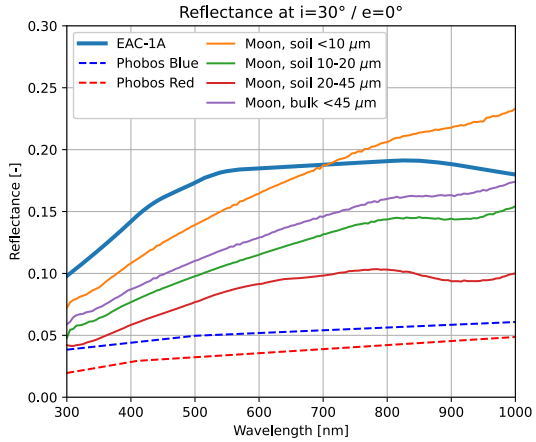

Fig. 3. From [6]: Reflectance properties of Phobos and the Moon (Apollo 14 sample 14163) compared to the EAC-1A analog soil. The Phobos values are predictions from [5]. The expected standard reflectance is at an incidence angle $i = 30°$ and an emission angle $e = 0°$.

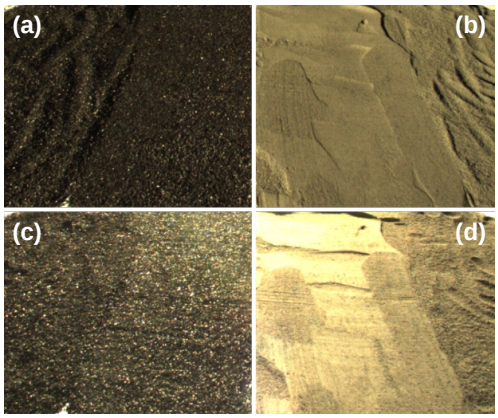

Fig. 4. Reflectance examples under different illumination angles. A very dark metallurgical coke (87% carbon) sample is shown in (a) and (c), and the EAC-1A in (b) and (d). In all cases, half of the sample surface is smoothed. One can see that (b) and (c) feature similar image illumination despite having highly different reflectance and grain size properties. For (a) and (b), the illumination is at an azimuth and elevation of (-110°, 15°), and for (c) and (d) at (0°, 15°).

B. Testing for NAVDLR

A successful performance of NAVDLR in the mission can only be guaranteed by thorough testing as described in [6]. Most data recording and live tests are performed in the DLR Planetary Exploration Laboratory (PEL). It is a $10\,\mathrm{m} \times 5\,\mathrm{m}$ sand bed, currently filled with the Moon analog material EAC-1A [20], which can be seen in Fig. 1. Its optical properties were determined by [6] and are shown in Fig. 3. An onboard view of the scene is shown in Fig. 2-a.

PEL has black molton curtains to cover the background and minimize stray light. It has two strong, interchangeable light sources meant to emulate the Sun. The illumination does not reach the Sun's levels, but given that the EAC-1A is brighter than the Phobos soil, we assume these effects to cancel out approximately. Finally, PEL features an ARTracking[1] motion capture system that allows us to record a precise ground truth reference trajectory as six-dimensional poses in space.

One of the recorded data sets forms the baseline for our evaluation in this paper. The respective trajectory is plotted in Fig. 5. The data set was recorded with a commercial off-the-shelf (COTS) camera setup that is similar to the flight model and is shown in Fig. 1. It features the same CMV4000 chip as the flight system with a pixel pitch of $5.5 \times 5.5\,\mu\mathrm{m}$ that records images at a 2048×2048 resolution and with a horizontal baseline of $60\,\mathrm{mm}$, see [6] for details.

C. Risks for NAVDLR

In general, both SGM and VO process the camera images directly and aim to find corresponding pixels between camera images. Thus, a degradation in image quality will directly result in a worse performance of SGM and VO and subsequently all other NAVDLR modules, making them the most relevant steps for this paper. However, SGM leverages a-priori information like the stereo camera calibration to constrain the pixel-correspondence searches on 1D lines. We assume that this makes SGM less likely to suffer from pixel noise.

Contrarily, the VO has much less prior information about correspondences available. In a given left camera image, it computes corner features [4] (i.e., pixels with strong gradients in both image coordinate directions) and selects those pixels with the highest contrast score. For these features, the surrounding pixels' values function as *feature descriptors* [4]. The same is done for the subsequent image, and all feature descriptors are searched to create matching correspondences that allow the computation of the ego-motion of the camera between the images as a 6D pose.

We consider VO to be most susceptible to the environment, as there is a high risk that a) not enough corner features are found due to the reduced contrast in dark images, b) the feature descriptors get corrupted due to noise, and c) wrong feature correspondences are detected due to hot pixels or other noise.

IV. Environment and Radiation Effects on Camera Images

NAVDLR's SGM and VO algorithms depend on finding correspondences between images, which assumes consistent conditions during image capture. However, factors like stereo camera decalibration, vignetting, motion blur, exposure differences, and lens flares can affect image quality and limit performance. While many of these issues can be addressed through calibration, the study focuses on three key effects – illumination, temperature, and radiation – that are particularly relevant to the Phobos environment and impact the camera's signal-to-noise ratio.

[1] https://ar-tracking.com

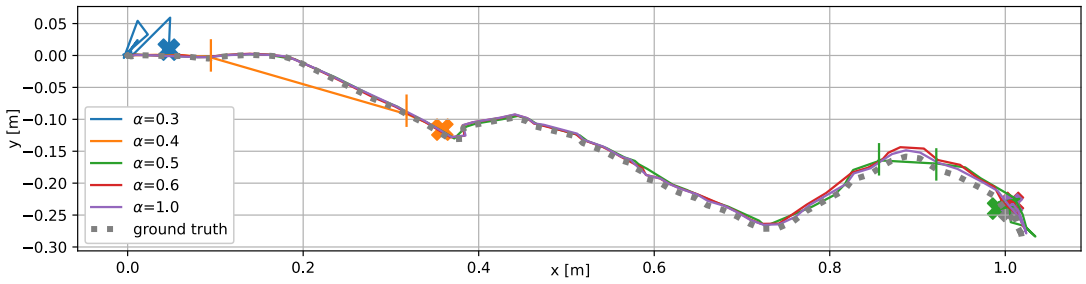

Fig. 5. Navigation results of NAVDLR for the illumination variation test. α is the scaling factor of the image brightness. Loss- and recapture-of-tracking are highlighted by vertical bars.

A. ILLUMINATION

Phobos is part of the Martian system and therefore receives significantly less sunlight than the Earth system. The distance from Phobos to the Sun oscillates between approximately 1.4 and $1.65\,\mathrm{AU}$ [5], reducing the illumination by a factor of 0.5 to 0.35 compared to the sunlight received on top of Earth's atmosphere.

In [6], we provide an overview of the Phobos reflectance estimate together with references to the Moon as shown in Fig. 3. The reflectance estimates are obtained from [5] and provide different values for a "red" and a "blue" part of the Phobos surface. This color-naming is only subtle as the surface of Phobos is generally very dark, significantly darker than the Moon [1], as shown in Fig. 3. However, there is a high uncertainty on Phobos' surface structure with the real distribution properties of the soil particle sizes unknown [12]. Fig. 3 also shows how the effective sunlight reflectance depends on grain size - in this case, measured for the Moon. Similarly, Fig. 4 illustrates how identical soil samples can appear highly different in a camera image with identical settings, if the incidence angle of the Sun or the surface composition changes.

This means that NAVDLR will encounter unknown and potentially highly variable illumination conditions on Phobos. In general, a camera image is the integral of the Photon flux to each pixel over time. Thus, even very dark scenes can appear bright given a long enough exposure time.

This results in a trade-off between a possible rover motion speed and the requirement to obtain images with a sufficient illumination but without motion blur. For the case of IDEFIX, this is especially important, as the wheel grousers (see Fig. 1) are big "shovels" optimized for traction in loose soil, but can induce significant body motions on compacted soil or while driving over stones, as they act more like a polygon than a round wheel in these cases. This causes a camera rotation motion, which is usually more prone to creating motion blur than linear forward camera motions.

It is a key aspect of our evaluation to see to what extent we can feed images with short exposure times (i.e., low-illuminated images) to our navigation pipeline while still achieving a satisfactory navigation accuracy. As a simplified approach, we assume a linear scaling of the reflectance curves for the resulting image brightness and modify all pixel intensity values I_{data} of the test data equally with a scaling factor α as $I_{\text{phobos}} = \alpha \cdot I_{\text{data}}$.

B. TEMPERATURE

The camera chip is generally subjected to an underlying measurement noise, consisting of multiple elements such as the so-called *Photon shot noise* or the *dark current*, among others [22]. The dark current elements consist of thermally generated electrons and are dependent on the sensor's temperature [22]. This is due to the increased interaction of incident particles with the silicon lattice of the sensor at elevated temperatures, which leads to both higher shot noise (an effect which can also be experienced on Earth) and an amplified radiation-induced dark current [23].

The IDEFIX rover will experience intense temperature cycles as Phobos' surface temperature varies from $60\,\mathrm{K}$ to $330\,\mathrm{K}$ [12]. We therefore simulate different temperature scenarios to understand the influence on the image quality. Note that the data recording occurred at room temperatures; thus, the reference images are already subject to temperature-based noise, where the simulated noise is added to. Therefore, our analysis has the potential to overestimate the temperature risks.

C. RADIATION

Radiation is the final environmental aspect that we will consider. Lacking an atmosphere or a magnetic field, Phobos is exposed to the radiation conditions of interplanetary space, causing image effects as illustrated by Fig. 6.

The radiation effects cause an increase in dark current on the camera chip, leading to higher noise levels. Goiffon [24] summarizes the radiation-induced dark current on silicon sensors comprehensively. The radiation dose induced into an electronic device can be quantified as the stopping power, or energy loss per unit length of a charged particle passing through a material, consisting of a proportion of ionizing energy loss (Linear Energy Transfer, LET) and a proportion of non-ionizing energy loss (NIEL).

The total ionizing dose (TID), which measures the cumulative amount of ionizing radiation energy absorbed by a material over time, is calculated as the product of LET and the particle fluence, i.e., the accumulated number of

Original Image	Shot Noise	TID Dark Current	CosmiX Proton Ray	Displacement Damage	Combined
Parameter	313 K	400 e^-/s for 5 krad	600 $cm^{-2}s^{-1}$	40 TeV/g	
PSNR / MSSIM	45.3 / 99.7%	44.2 / 99.2%	32.1 / 92.4%	22.6 / 74.1%	21.6 / 68.9%

Fig. 6. Simulated noise effects for the "worst case" scenario. The *structural difference* between images [21] of Pyxel-modified images and the original non-irradiated image is shown. Peak signal-to-noise-ratio (PSNR) and Mean Structural Similarity (MSSIM) [21] illustrate the degraded image quality.

particles. Similarly, the displacement damage dose (DDD), which measures the non-ionizing energy transferred to atoms in a material, causing displacement defects, is defined as the product of NIEL and the particle fluence.

Radiation will cause two principal cumulative effects on the MMX rover camera. First, the TID and DDD will increase the dark current across all pixels, leading to elevated sensor noise [16]. Second, the DDD will result in a higher count of hot pixels (abnormally bright pixels due to lattice defects and current leakage) on the camera chip.

Additionally, instantaneous and transient effects can be visible in the camera image due to cosmic rays. These are caused by high-energy particles that strike the camera and directly deposit charge on the camera sensor, causing streaks in the camera image [25], as simulated in Fig. 6.

Finally, a shielding of the camera chip can reduce the incoming radiation and is quantified as *thickness of aluminium*.

V. METHODOLOGY

To study the environmental effects on the navigation performance of NAVDLR, we create the following pipeline, where we modify a pre-recorded navigation image sequence from our PEL facility, re-run it with NAVDLR, and use the high-accuracy ground truth as reference.

A. RADIATION AND TEMPERATURE SIMULATION

Pyxel [18] is a Python-based simulation framework for imaging detectors, developed to integrate and combine various models that simulate instrument effects. It is a tool developed by ESA that allows the simulation-based generation of new images from photon sources or the alteration of existing images by overlaying radiation noise in accordance with the camera sensor type and the expected character of space radiation. As it can be used as a post-processing tool, we alter our existing test data sets and compare the change in navigation accuracy with added radiation influence.

WWe use Pyxel to simulate the charge deposition from cosmic rays (Pyxel's CosmiX model), charge diffusion, readout noise, and radiation-induced dark current in CMOS-based imaging detectors. Pyxel can also take the temperature of the CMOS sensor into account.

B. DATA SET MODIFICATION

The raw dataset underwent a series of modifications to incorporate the discussed effects, as shown in Fig. 7:

1) The scaling α adjusts the brightness level of the stereo images.
2) A noise mask simulating DDD-induced hot pixels is created using Pyxel's *Radiation Induced Dark Current Model* on a black background. Separate masks are created per camera (left and right) and kept consistent for the respective camera over each evaluation run.
3) For each readout, cosmic ray tracks from the CosmiX Proton Ray Irradiation Model, temporary TID-induced dark current, and shot noise are added to a second noise mask that is individual for each image of each camera.
4) The noise masks are combined and applied to the brightness-modified raw stereo images.
5) The noise-modified images are then demosaiced, rectified, and binned to create 8-bit stereo image pairs for use by NAVDLR.

VI. TESTS

Two sets of tests were conducted to study the performance of the NAVDLR autonomous navigation software under

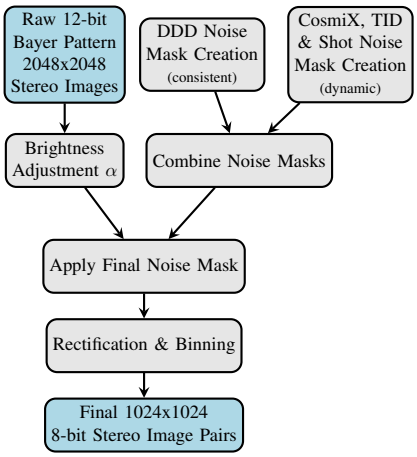

Fig. 7. Data set modification process flow chart.

Phobos-like conditions: one for illumination and the second for all combined environmental effects. All tests were carried out on a data set with a one-meter-long trajectory involving translational and rotational movements as shown in Fig. 5.

A. Test Scenarios

a) Illumination: The initial series of tests aims to evaluate the impact of reduced illumination levels on the performance of NAVDLR. Recall from Section IV-A tthat we expect a substantial variation in effective illumination conditions w. r. t. the resulting camera image brightness. To test this, we reduce the brightness of the data set linearly to simulate the low-light conditions expected on Phobos. The navigation software runs five times, each with a different illumination scaling $\alpha \in \{0.3, 0.4, 0.5, 0.6, 1.0\}$.

b) Illumination, Temperature, and Radiation combined: The other and more comprehensive test series simulates the combined effects of the multiple environmental factors illumination, radiation (ionizing and non-ionizing), temperature-dependent shot noise, and cosmic ray influences. The combined tests were performed under two scenarios, obtained from [26][2]:

- *Nominal scenario*: simulating expected space radiation conditions throughout the MMX mission. This includes a dark current rate of $250\,\mathrm{e^-/s}$ (TID $= 1\,\mathrm{krad}$), $20\,\mathrm{TeV/g}$ (at $5\,\mathrm{Al\,mm}$ shielding) for DDD, and a $6\,\mathrm{cm^{-2}{\cdot}s^{-1}}$; $100\,\mathrm{MeV}$ proton equivalent for the cosmic rays.
- *Worst-case scenario*: representing extreme conditions with higher radiation doses and cosmic ray impacts during the worst week of a solar flare. This includes a dark current rate of $400\,\mathrm{e^-/s}$ (TID $= 5\,\mathrm{krad}$), $40\,\mathrm{TeV/g}$ (at $3\,\mathrm{Al\,mm}$ shielding) for DDD, and a $600\,\mathrm{cm^{-2}{\cdot}s^{-1}}$; $100\,\mathrm{MeV}$ proton equivalent for the cosmic rays.

For both scenarios, three different illumination levels $\alpha \in \{0.5, 0.6, 1.0\}$ are tested, alongside two operating temperatures $T \in \{273\,K, 313\,K\}$. This results in 12 test runs $\{\text{nominal case}, \text{worst case}\} \times \alpha \times T$.

To illustrate the effects of the individual radiation parameters, Fig. 6 shows subtracted negative images of individual effects simulated by Pyxel. Here, we use the peak signal-to-noise ratio and the mean structural similarity [21] to quantify the impact of the individual factors on the image quality.

B. Metrics

We evaluate the robustness of NAVDLR using several metrics. First, we evaluate if VO was able to estimate the whole trajectory or if a *loss of tracking* occurred. A temporary loss of tracking happens, when VO can not establish a correspondence of a minimum of features between the current image and one of the stored five key frames, but VO might recover the correspondence using subsequent images. A permanent loss of tracking happens, when no recovery was possible.

We furthermore use the absolute trajectory error (ATE) to assess how much the trajectory deviates from the ground truth in absolute terms. Similarly, we use the relative pose error (RPE), which allows us to compare the relative error in the pose increments. We consider both metrics as mean-normalized over the trajectory, require values of less than $3\,\%$ to consider a navigation run as *accurate*, and assume that error variations within $1\,\%$ are noise.

These are frequently used metrics, and we provided a more detailed summary of them in [27]. The tool *evo*[3] provides built-in functionalities for trajectory evaluation, which we use here for our evaluation.

TABLE I

COVERED DISTANCE AND MEAN NORMALIZED RPE AND ATE OF THE ILLUMINATION TEST SERIES.

α	coverage	RPE	ATE
1.0	100%	0.94%	1.28%
0.6	100%	1.18%	1.30%
0.5	99%	1.39%	1.56%
0.4	28%	1.92%	1.19%
0.3	0%	-	-

VII. RESULTS

We run our NAVDLR pipeline on both test scenarios and apply the evaluation metrics on the results.

A. Evaluating the Illumination Impact

The results of the first test scenario are shown in Fig. 5, and the metrics are listed in Table I. The pose errors are minor, and an *accurate* navigation can generally be expected. However, reaching dark levels of $\alpha \leq 0.4$, the VO can find feature correspondences to some extent, but suffers an irrecoverable *loss of tracking* eventually. Figure 5 shows that during $\alpha = 0.4$, VO can recover from its first loss of tracking after a few images thanks to its key-frame history. Similarly, $\alpha = 0.5$ briefly loses tracking at the last turn – presumably due to a fast camera rotation – but can recover immediately. Thus, for NAVDLR, minimum effective image illumination is required to enable robust navigation results.

B. Evaluating the Combined Impact

Finally, NAVDLR's results with the combined effects of environmental factors are listed in Table II and shown in Fig. 8. Generally, the *accuracy* of NAVDLR is satisfactory. However, it suffers a loss of tracking in the more challenging cases.

At constant radiation and illumination levels, the pose estimation fails at higher temperatures in nearly all cases before completing the trajectory, indicating that the temperature-related noise highly influences NAVDLR. The dependency on the illumination conditions remains similar to that in our

[2]Note that we present slightly altered values due to disclosure restrictions.

[3]https://github.com/MichaelGrupp/evo

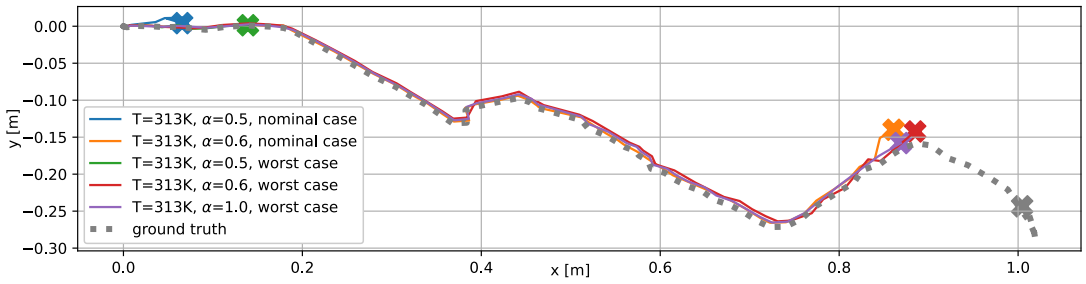

Fig. 8. *Unsuccessful* navigation results of NAVDLR for the combined variation test, looking at illumination α, temperature T, and the two defined radiation scenarios. The seven runs that completed the trajectory are omitted for better visibility.

first test scenario. There is no significant increase in the error rate when directly comparing the "nominal case" to the "worst case" radiation scenarios. As the radiation noise has predominantly local effects in the image, we assume that NAVDLR's *binning* operation from 2048×2048 to 1024×1024 operates as a low-pass filter on the image, as it averages and combines four adjacent pixels into one, thus smoothing out many radiation effects.

Fig. 8 shows that the navigation fails at approximately the same location for three test cases (nominal, 0.6, 313 K), (worst case, 0.6, 313 K), and (worst case, 1.0, 313 K). This is the same turn where $\alpha = 0.5$ from the first test briefly loses tracking. It indicates that this is a generally challenging navigation moment for NAVDLR, and increased background noise increases the likelihood of losing tracking. Conversely, commanding slower and more conservative motions to the rover would increase the likelihood of a successful navigation.

The most influential parameters, temperature and illumination, can be actively controlled during rover operations. The former can be achieved, e.g., by scheduling the drives in the morning. The latter requires higher camera exposure times for mitigation, potentially restricting the rover's motion speed. These techniques would therefore introduce operational constraints as a downside.

Finally, we conclude that under the nominal radiation conditions with sensors maintained at low temperatures and brightness levels above 0.5 relative to the test data, a failure of the navigation software in its current form is unlikely.

VIII. SUMMARY

The NAVDLR algorithm can be considered well-suited for the assumed environmental conditions of this paper, which closely correlate with the expected but yet uncertain Phobos conditions. It is always able to perform *accurate* navigation w. r. t. the given metrics. In the more extreme cases, a loss of tracking occurs. This behavior is desirable, as a loss of tracking constitutes a clearly defined error case that can be detected, and error mitigation processes can be started. In contrast, a gradual deterioration in the navigation accuracy is challenging to detect and would pose a high risk to the rover. The sensor temperature and illumination influences could be mitigated by adapted rover operations, e.g., driving during the morning of a Phod, if necessary. Regarding the radiation noise, we assume that the binning of the camera images filters out many radiation effects on the camera and thus reduces the risk of spurious feature detection and matching.

TABLE II

COVERED DISTANCE OF THE TRAJECTORY AND MEAN NORMALIZED RPE AND ATE OF THE ALL-COMBINED TEST SERIES.

T	α	Nominal Dose coverage	Nominal Dose RPE	Nominal Dose ATE	Worst Case Dose coverage	Worst Case Dose RPE	Worst Case Dose ATE
273K	1.0	100%	1.11%	1.22%	100%	1.02%	1.02%
	0.6	100%	1.09%	1.25%	100%	0.94%	1.08%
	0.5	100%	1.31%	1.33%	100%	0.99%	1.37%
313K	1.0	100%	0.97%	1.21%	82%	1.77%	1.61%
	0.6	86%	1.38%	1.77%	86%	1.68%	1.64%
	0.5	6%	5.69%	4.87%	9%	2.40%	3.40%

This study is meant as an initial proposal to study the effects of illumination, temperature, and radiation on vision-based algorithms, as it is limited in scope and the multitude of parameters and effects that were studied. Future work is needed to dive deeply into the camera effects expected in deep space and evaluate the individual steps in vision algorithms concerning this. Additionally, it would be fruitful to study existing terrestrial navigation solutions and identify those that are potentially most robust by design. This becomes especially relevant in scenarios where even higher radiation or less sunlight is expected, e.g., for exploring the Jovian moons or for terrestrial applications in hazardous radiation environments.

REFERENCES

[1] K. Kuramoto, Y. Kawakatsu, M. Fujimoto, *et al.*, "Martian Moons Exploration MMX: Sample return mission to Phobos elucidating formation processes of habitable planets," *Earth, Planets and Space*, vol. 74, no. 1, 2022.

[2] Y. Kawakatsu, K. Kuramoto, T. Usui, *et al.*, "Launch year change of Martian Moons Exploration (MMX) and its recent status," in *75th International Astronautical Congress*, Milan, Italy, 2024.

[3] P. Michel, S. Ulamec, U. Böttger, *et al.*, "The MMX rover: Performing in situ surface investigations on Phobos," *Earth, Planets and Space*, vol. 74, no. 1, 2022.

[4] M. Vayugundla, T. Bodenmüller, L. Burkhard, *et al.*, "The DLR autonomous navigation experiment with the IDEFIX rover: Software architecture, autonomous navigation features and preliminary operations concept," in *2025 IEEE Aerospace Conference*, IEEE, Mar. 2025, pp. 1–20.

[5] S. Tardivel, J. Biele, F. Buse, *et al.*, "Phobos Environment Requirement Document for the MMX rover mission," CNES, DLR, et al., Tech. Rep., Sep. 5, 2019, Internal.

[6] L. Meyer, M. Vayugundla, P. Kenny, *et al.*, "Testing for the MMX rover autonomous navigation experiment on Phobos," in *2023 IEEE Aerospace Conference*, 2023, pp. 1–19.

[7] M. Maimone, Y. Cheng, and L. Matthies, "Two years of visual odometry on the Mars Exploration Rovers," *Journal of Field Robotics*, vol. 24, no. 3, pp. 169–186, 2007.

[8] M. Maimone, N. Patel, A. Sabel, A. Holloway, and A. Rankin, "Visual odometry thinking while driving for the Curiosity Mars Rover's three-year test campaign: Impact of evolving constraints on verification and validation," in *2022 IEEE Aerospace Conference*, 2022, pp. 1–10.

[9] R. Rieber, M. McHenry, P. Twu, and M. M. Stragier, "Planning for a Martian road trip - the Mars2020 mobility systems design," in *2022 IEEE Aerospace Conference*, 2022, pp. 1–18.

[10] J. Wang, J. Li, S. Wang, *et al.*, "Computer vision in the teleoperation of the Yutu-2 rover," *ISPRS Annals of Photogrammetry, Remote Sensing and Spatial Information Sciences*, vol. V-3-2020, pp. 595–602, Aug. 2020.

[11] R. Soussan, J. McCaffery, S. McMichael, and M. Deans, "Luvo: Lunar visual odometry using homography-based image feature matching," in *2025 IEEE International Conference on Robotics and Automation*, IEEE, May 2025, pp. 13 428–13 435.

[12] H. Miyamoto, T. Niihara, K. Wada, *et al.*, "Surface environment of Phobos and Phobos simulant UTPS," *Earth, Planets and Space*, vol. 73, Dec. 2021.

[13] D. A. Lorenz, R. Olds, A. May, *et al.*, "Lessons learned from OSIRIS-REx autonomous navigation using natural feature tracking," in *2017 IEEE Aerospace Conference*, IEEE, Mar. 2017, pp. 1–12.

[14] F. Scholten, F. Preusker, S. Elgner, *et al.*, "The Hayabusa2 lander MASCOT on the surface of asteroid (162173) Ryugu – stereo-photogrammetric analysis of MASCam image data," *Astronomy and Astrophysics*, vol. 632, p. L5, Dec. 2019.

[15] C. Virmontois, O. Gasnault, S. Maurice, *et al.*, "Color CMOS-based microcamera for space exploration," in *47th Annual Lunar and Planetary Science Conference*, 2016, p. 2862.

[16] C. Virmontois, J.-M. Belloir, M. Beaumel, *et al.*, "Dose and single-event effects on a color CMOS camera for space exploration," *IEEE Transactions on Nuclear Science*, vol. 66, no. 1, pp. 104–110, 2019.

[17] J. Poravanthattil, D. C. Stumpp, S. Roffe, and A. D. George, "Fault mitigation for SNN classification of neuromorphic event streams with radiation-induced noise," in *2025 IEEE Aerospace Conference*, IEEE, Mar. 2025, pp. 1–14.

[18] D. Lucsanyi, T. Prod'homme, H. Smit, *et al.*, "Pyxel: a novel and multi-purpose Python-based framework for imaging detector simulation," in *High Energy, Optical, and Infrared Detectors for Astronomy VIII*, A. D. Holland and J. Beletic, Eds., International Society for Optics and Photonics, vol. 10709, SPIE, 2018, pp. 325–333.

[19] H. Hirschmüller, "Accurate and efficient stereo processing by semi-global matching and mutual information," in *CVPR 2005*, vol. 2, IEEE, Jun. 2005, pp. 807–814.

[20] V. Engelschiøn, S. Eriksson, A. Cowley, *et al.*, "EAC-1A: A novel large-volume lunar regolith simulant," *Scientific Reports*, vol. 10, p. 5473, Mar. 2020.

[21] Z. Wang, A. Bovik, H. Sheikh, and E. Simoncelli, "Image quality assessment: From error visibility to structural similarity," *IEEE Transactions on Image Processing*, vol. 13, no. 4, pp. 600–612, Apr. 2004.

[22] M. Konnik and J. Welsh, "High-level numerical simulations of noise in CCD and CMOS photosensors: Review and tutorial," *arXiv*, 2014.

[23] J. Srour and D. Lo, "Universal damage factor for radiation-induced dark current in silicon devices," *IEEE Transactions on Nuclear Science*, vol. 47, no. 6, pp. 2451–2459, 2000.

[24] V. Goiffon, "Radiation effects on CMOS active pixel image sensors," *Ionizing Radiation Effects in Electronics*, 2015.

[25] D. Lucsányi and T. Prod'homme, "Simulating charge deposition by cosmic rays inside astronomical imaging detectors," *IEEE Transactions on Nuclear Science*, vol. 67, no. 7, pp. 1623–1628, 2020.

[26] D. Standarovski, N. Balcon, J. Mekki, and S. Mary, "MMX small rover radiation environment specification," CNES, Tech. Rep., Jan. 21, 2020, Internal.

[27] L. Meyer, M. Smíšek, A. Fontan Villacampa, *et al.*, "The MADMAX data set for visual-inertial rover navigation on Mars," *Journal of Field Robotics*, vol. 38, no. 6, pp. 833–853, 2021.